Precambrian Research 169 (2009) 58–67

Contents lists available at ScienceDirect

Precambrian Research

journal homepage: www.elsevier.com/locate/precamres

Lithofacies control on multiple-sulfur isotope records and Neoarchean sulfur cycles

Shuhei Ono[a,*], Alan J. Kaufman[b], James Farquhar[b], Dawn Y. Sumner[c], Nicolas J. Beukes[d]

[a] Department of Earth, Atmospheric, and Planetary Sciences, Massachusetts Institute of Technology, 77 Massachusetts Avenue, Cambridge, MA 02139-4307, USA
[b] Department of Geology and Earth System Science Interdisciplinary Center, University of Maryland, College Park, MD 20742, USA
[c] Department of Geology, University of California, 1 Shields Ave, Davis, CA 95616, USA
[d] Department of Geology, University of Johannesburg, 2006 Auckland Park, South Africa

ARTICLE INFO

Article history:
Received 30 October 2007
Received in revised form 7 January 2008
Accepted 23 October 2008

Keywords:
Mass-independent fractionation
Sulfur isotope
Archean
Atmosphere
Transvaal
Agouron
Neoarchean
Oxygen
S-33
Multiple-sulfur isotope

ABSTRACT

Triple-sulfur isotope ratios ($^{32}S/^{33}S/^{34}S$) were measured for 141 bulk rock samples from two Agouron scientific drill cores (GKP01 and GKF01) that recovered Neoarchean successions of the Transvaal Supergroup, South Africa. These two deep-time cores are correlated to each other with 14 tie lines using volcanic and impact spherule layers in a sequence stratigraphic framework, allowing us to evaluate both lithofacies and temporal controls over multiple-sulfur isotope systematics. The ca. 2.5 Ga (giga-annum before present) basinal Klein Naute Formation and the ca. 2.6 Ga peritidal Boomplaas and Vryburg Formations yield an array of data characterized by $\delta^{33}S \approx 1.4 \times \delta^{34}S$. These linear trends are found in both shallow water and deepwater facies but are characteristic to rocks with high-iron content suggesting these may reflect isotopic compositions of aqueous sulfide-elemental sulfur reservoirs in the Neoarchean oceans.

Data that deviate from this linear array are interpreted as resulting from additional inputs of sulfide from microbial sulfate reduction with or without contribution from sulfur disproportionation. Sulfate-derived sulfur evolved to be either enriched or depleted in ^{34}S depending on the local depositional environment. For example, the Reivilo Formation in core GKF01 is characterized by abundant microbialite textures and shows an isotopic signature of closed system sulfate reduction. Rapid cementation of these carbonate fabrics may have attenuated the supply of sulfate to pore waters resulting in the progressive ^{34}S enrichments during bacterial sulfate reduction below the sediment–water interface. In contrast, signatures of open-system sulfate reduction are associated with slope facies, dominated by granular dolostones, preserved in the upper Nauga Formations in GKF01 and GKP01. The two different sulfur isotope patterns, interpreted to reflect closed versus open-system sulfate reduction are both found in the lower Reivilo Formation in both cores. This lateral variation of isotope signals documents that observed ^{34}S shifts can be controlled locally, and may not have temporal significance. This study demonstrates critical importance of recovering sulfur isotope data from stratigraphically correlated drill cores to evaluate both geographical and temporal shifts of sulfur cycles, and their links to the great oxidation event at the end of the Archean Eon.

1. Introduction

Sulfur isotope ratios of Archean sulfide and sulfate minerals exhibit signatures of mass-independent fractionation (S-MIF) that are measured as deviations from mass-dependent relationships among three isotope ratios of sulfur (i.e., $\delta^{33}S \neq 0.515\ \delta^{34}S$ and $\delta^{36}S \neq 1.9\ \delta^{34}S$), which result in non-zero $\Delta^{33}S$ and $\Delta^{36}S$ values.[1] The S-MIF signatures are thought to have originated from sulfur photochemical reactions in an anoxic atmosphere, and disappear from the rock record during the early Paleoproterozoic due to oxygenation of the atmosphere (Farquhar et al., 2000; Pavlov and Kasting, 2002; Bekker et al., 2004).

The existing Neoarchean S-MIF records are characterized by large apparent stratigraphic variations of $\Delta^{33}S$ values (−2.5 to +11.2‰; Ono et al., 2003; Kamber and Whitehouse, 2007; Kaufman et al., 2007). These large $\Delta^{33}S$ variation may provide new insights into how the rise of atmospheric oxygen occurred during the Paleoproterozoic Era (e.g., Ono et al., 2003; Eigenbrode and Freeman, 2006; Kaufman et al., 2007; Anbar et al., 2007). Kaufman et al. (2007) presented high-resolution triple-sulfur isotope analysis for 90 m sections of the drill core, ABDP-9, from Western Australia. The one-dimensional trend recorded in individual core remains to be

* Corresponding author. Tel.: +1 617 253 0474; fax: +1 617 253 8630.
E-mail address: sono@mit.edu (S. Ono).

[1] Sulfur isotope values are reported using the conventional delta notation: $\delta^x S = ({}^xR_{sample}/{}^xR_{VCDT} - 1) \times 1000$ (‰), where ${}^xR$ is the isotope ratio, ${}^xS/{}^{32}S$ ($x = 33$ or 34), of the sample and VCDT (Vienna-Cañyon Diablo Troilite). Capital delta values are defined as (Farquhar et al., 2000): $\Delta^{33}S = \delta^{33}S - 1000 \times [(1 + \delta^{34}S/1000)^{0.515} - 1]$.

0301-9268/$ – see front matter © 2009 Elsevier B.V. All rights reserved.
doi:10.1016/j.precamres.2008.10.013

rigorously tested in a sequence stratigraphic and sedimentologic framework.

In an anoxic Archean atmosphere, aerosols of both S_8 and H_2SO_4 would have deposited on the ground and in the oceans. This contrasts with today's oxic atmosphere, where atmospheric sulfur exits almost exclusively as H_2SO_4 aerosols (Kasting et al., 1989; Farquhar et al., 2000; Pavlov and Kasting, 2002). It is suggested that S_8 carried positive $\Delta^{33}S$ signals, whereas H_2SO_4 carried negative $\Delta^{33}S$ signals into the oceanic sulfur reservoirs (Farquhar et al., 2000, 2001; Ono et al., 2003). These distinct $\Delta^{33}S$ signals were transferred into sedimentary sulfides after biological and/or inorganic processing in the oceans. Thus, stratigraphically resolved analysis of multiple-sulfur isotope systematics in relation to sedimentary facies allows us to trace oceanic Archean sulfur cycles and key microbial processes (Ono et al., 2003; Kamber and Whitehouse, 2007; Kaufman et al., 2007).

Here, we report triple-sulfur isotope ratios ($\delta^{33}S$ and $\delta^{34}S$) of sulfur from bulk rock powders and from extracted sulfides from two long (>1 km length) scientific drill cores representing both platform slope and basinal environments. The use of a rapid, high-throughput elemental analyzer-isotope ratio mass spectrometry (EA-IRMS) technique (Baublys et al., 2004; Kaufman et al., 2007) enabled the analysis of samples collected in several tens of meters interval for the entire length of the two long drillcores. The analysis of correlative intervals with different lithofacies provides an improved understanding of the effects of lithofacies on triple-sulfur isotope abundances. It is critically important to resolve geographical control on sulfur isotope systematics prior to attributing any stratigraphic trends to the evolution of sulfur biogeochemical cycles and its link to the early evolution of life, atmospheric and ocean chemistry.

2. Geologic setting

The lower Transvaal Supergroup consists of a mixed siliciclastic-carbonate ramp that grades upward into an extensive carbonate platform overlain by banded iron-formation. It was deposited on the Kaapvaal Craton between 2.67 and 2.46 Ga (Armstrong et al., 1986; Barton et al., 1994; Sumner and Bowring, 1996; Walraven and Martini, 1995), with subsidence driven by cooling of the craton after extrusion of the 2.7 Ga Ventersdorp flood basalts (Figs. 1 and 2; Sumner and Beukes, 2006). The ramp to platform is up to 2-km thick, with predominantly peritidal facies in the north and east and deeper facies to the south and west (Beukes, 1987; Sumner and Beukes, 2006; Sumner and Grotzinger, 2004). Platform, slope and basinal sediments are preserved between Griquatown and Prieska (Beukes, 1987; Sumner and Beukes, 2006). The sequence stratigraphic framework of this ramp-to-platform transect has been well documented, providing numerous time-lines from peritidal to deep subtidal depositional environments (Sumner and Beukes, 2006, and references therein).

Two Agouron Institute scientific drill cores GKP01 (S 28°56′06.0″ E 023°15′0.00″) and GKF01 (S 29°08′12.5″ E 23°08′06.9″), were drilled through slope facies to provide fresh rock samples for geochemical analysis. The 2 cores are correlated to each other with 14 tie lines using volcanic and impact spherule layers and distinctive facies distributions (Figs. 1 and 2; Schröder et al., 2006; Sumner and Beukes, 2006). Water depths represented in the cores range from near wave base to hundreds of meters with GKP01 representing deeper facies than GKF01.

The cores intersected, from the lowest, the Vryburg, Boomplaas, Lokammona Formations of the Schmidtsdrif Supergroup, and the Monteville, Reivilo or lower Nauga, upper Nauga, and Klein Naute Formations of the Campbellrand Supergroup, and the lowermost part of the Kuruman Iron Formation of the Asbestos Hill Supergroup (Fig. 2). Here, we refer to the lower Nauga Formation as the Reivilo Formation because the facies in the core are more similar to the Reivilo Formation than the formally defined Nauga Formation (Fig. 2; see Beukes, 1987; Sumner and Beukes, 2006). The sequence boundary between the Reivilo and the upper Nauga Formations is defined by the Kamden Member marker bed, identical with that defined by Schröder et al. (2006) for the lower and upper Nauga Formations.

We will discuss the triple-sulfur isotope systematics by subdividing the studied cores into seven sections by major change of lithofacies as they indicate change in depositional environment, such as water depth. Our seven sections are, from the lowest, the Vryburg (VB), Boomplaas (BP), Lokammona and Monteville (LM), Reivilo and a part of upper Nauga (RN1), and the rest of upper Nauga (N2), lower Klein Naute (KN1), and upper Klein Naute and lower Kuruman (KN2K) intervals (Fig. 4). In our subdivision, a part of the lower upper Nauga Formation (525–675 m in GKP01 and 785–897 m in GKF01) is grouped with the Reivilo Formation, and called RN1, because dominant lithology changes from microbialite to slope dolostone at these stratigraphic intervals (at ca. 785 m for GKF01 and ca. 525 m for GKP01; Figs. 3 and 4). The Reivilo and upper Nauga Formations of GKF01 are much thicker (ca. 1000 m) than those in GKP01 (625 m), indicating a steep depth gradient during deposition of these sections between the two cores (Fig. 4; Sumner and Beukes, 2006). The subdivision within the Klein Naute Formation corresponds to the lithologic change from carbonate and shale to iron formation, which occurs at ca. 280 m at GKP01 and 275 m at GKF01. This interval is tentatively correlated to the upper and lower Mt. McRae Shale, where a "whiff of oxygen" is suggested from the analysis of equivalent Australian cores (Kaufman et al., 2007; Anbar et al., 2007).

3. Analytical methods

A total of 135 shale samples with finely disseminated pyrite, 68 from GKP01 and 67 from GKP01, and 6 tuff samples were selected for sulfur isotope analyses. Intervals rich in pyrite layers and nodules were avoided because their major and trace element geochemistry will be biased due to abundant pyrite contents. These pyrite nodules and layers often carry S-MIF signatures different from fine-grained pyrite analyzed in this study. Isotope systematics for different textures of pyrites are discussed in an accompanying paper (Ono et al., this volume). The petrography and major and trace element chemistry for most samples used by this study are reported in Schröder et al. (2006), and the isotope ratios for organic and carbonate carbon are reported in Fischer et al. (this volume). The drill core samples were finely powered in an agate vibratory disc mill in preparation for sulfur isotope and other geochemical analysis.

For the first sets of samples, sulfur was extracted from samples with Cr-reduction diffusion method (Hsieh and Yang, 1989), and precipitated as Ag_2S (Table 1). Isotope ratios were measured by a Eurovector elemental analyzer interfaced with a GV gas source isotope ratio-mass spectrometer at the stable isotope laboratory of the University of Maryland. The prepared Ag_2S was combusted on-line with equal amounts of V_2O_5 and a pulse of O_2 at 1030 °C. The ion beams of m/z 48, 49, and 50 were measured and integrated for isotope ratio measurements (Baublys et al., 2004). Details of the method and standardization are described as supplementary information in Kaufman et al. (2007).

A second set of samples was analyzed by direct combustion of acidified bulk powders. For the bulk powder analysis, sulfur contents were previously measured by XRF (Schröder et al., 2006), and used to calculate sample weighs in order to obtain a constant signal level. Sample rock powders (~1 g) were acidified to dissolve carbonate minerals by using 6N hydrochloric overnight at room

Table 1
Sulfur isotope ratios for the core GKP01.

Depth	Stratigraphy	Subdivision	Analysis[a]	Acid loss[b]	S (wt.%)[c]	$\delta^{33}S$ (‰)	$\delta^{34}S$ (‰)	$\Delta^{33}S$ (‰)
226.55	Kuruman Fm.	KN2K	Bulk	0.40	0.4	−1.5	−4.4	0.7
228.15	Kuruman Fm.	KN2K	Bulk	0.32	0.8	−1.7	−4.6	0.7
250.10	Kuruman Fm.	KN2K	Bulk	0.54	0.3	−1.6	−5.0	1.0
276.95	K. Naute Fm.	KN2K	Bulk	0.37	0.3	−2.1	−5.9	0.9
279.82	K. Naute Fm.	KN2K	Bulk	0.36	0.8	−2.5	−3.4	−0.8
292.20	K. Naute Fm.	KN1	Cr-red		0.1	−1.4	−4.7	1.0
299.90	K. Naute Fm.	KN1	Bulk	0.09	0.4	3.5	1.7	2.7
306.20	K. Naute Fm.	KN1	Bulk	0.18	0.4	3.0	3.1	1.4
360.7[d]	U. Nauga Fm.	Tuff	Cr-red		0.8	1.1	−0.8	1.5
413.63[d]	U. Nauga Fm.	Tuff	Cr-red		0.6	−5.9	−11.9	0.3
486.75	U. Nauga Fm.	N2	Bulk	0.29	0.5	1.7	−1.0	2.1
491.15	U. Nauga Fm.	N2	Cr-red		0.6	1.5	1.9	0.6
494.20	U. Nauga Fm.	N2	Cr-red		0.7	4.4	2.6	3.0
495.50	U. Nauga Fm.	N2	Bulk	0.49	0.7	4.4	1.6	3.5
499.32	U. Nauga Fm.	N2	Cr-red			2.6	0.2	2.5
506.20	U. Nauga Fm.	N2	Bulk	0.65	0.8	4.7	−0.8	5.1
506.57	U. Nauga Fm.	N2	Bulk	0.66	0.2	3.0	−1.5	3.8
515.95[d]	U. Nauga Fm.	Tuff	Cr-red		0.2	0.5	−0.2	0.6
574.76[d]	U. Nauga Fm.	Tuff	Cr-red			8.2	4.2	6.0
614.55	U. Nauga Fm.	RN1	Cr-red		0.4	1.8	0.5	1.6
626.00	U. Nauga Fm.	RN1	Cr-red			6.9	2.9	5.4
637.00	U. Nauga Fm.	RN1	Cr-red		1.0	9.5	11.8	3.4
640.30	U. Nauga Fm.	RN1	Cr-red		0.6	5.9	4.2	3.8
721.65	Reivilo Fm.	RN1	Cr-red		0.6	1.4	−1.5	2.2
733.40	Reivilo Fm.	RN1	Cr-red		0.5	−5.1	−10.3	0.2
738.95	Reivilo Fm.	RN1	Cr-red		0.1	1.7	−1.4	2.4
743.10	Reivilo Fm.	RN1	Cr-red		0.2	4.1	0.2	4.0
798.50	Reivilo Fm.	RN1	Cr-red		0.2	4.7	3.3	2.9
871.83	Reivilo Fm.	RN1	Cr-red		2.6	−5.0	−11.4	0.9
891.25	Reivilo Fm.	RN1	Cr-red			3.3	1.0	2.8
892.40	Reivilo Fm.	RN1	Cr-red		0.6	−3.4	−6.1	−0.2
965.10	Monteville Fm.	LM	Cr-red			7.6	6.0	4.5
970.75	Monteville Fm.	LM	Cr-red		2.0	4.3	5.2	1.6
974.05	Monteville Fm.	LM	Cr-red		0.3	2.6	1.7	1.7
980.00	Monteville Fm.	LM	Bulk	0.03	0.3	10.1	8.2	5.9
1012.1[d]	Monteville Fm.	Tuff	Cr-red			20.0	21.4	8.9
1016.90	Monteville Fm.	LM	Bulk	0.06	0.2	13.2	11.8	7.1
1019.90	Monteville Fm.	LM	Cr-red		0.2	7.8	9.3	3.0
1028.20	Monteville Fm.	LM	Bulk	0.06	0.3	9.5	6.5	6.1
1035.70	Monteville Fm.	LM	Cr-red		0.6	11.0	11.9	4.9
1047.70	Monteville Fm.	LM	Cr-red		4.4	0.6	1.5	−0.1
1061.15	Lokammona Fm.	LM	Bulk	0.11	0.6	7.8	4.2	5.6
1077.00	Lokammona Fm.	LM	Cr-red		0.3	9.3	7.2	5.7
1079.90	Lokammona Fm.	LM	Cr-red		0.2	7.7	5.6	4.8
1081.75	Lokammona Fm.	LM	Bulk	0.32	0.2	9.5	5.4	6.7
1087.80	Lokammona Fm.	LM	Cr-red		0.2	6.1	3.5	4.3
1110.45	Boomplaas Fm.	BP	Bulk	0.24	0.4	6.5	3.5	4.7
1114.70	Boomplaas Fm.	BP	Bulk	0.32	0.3	9.8	5.7	6.9
1121.20	Boomplaas Fm.	BP	Bulk	0.24	0.4	2.7	1.5	1.9
1129.65	Boomplaas Fm.	BP	Bulk	0.30	0.5	7.6	4.2	5.4
1144.80	Boomplaas Fm.	BP	Bulk	0.34	0.4	9.0	5.0	6.4
1150.90	Boomplaas Fm.	BP	Cr-red		0.2	6.8	4.5	4.5
1155.15	Boomplaas Fm.	BP	Cr-red		0.2	2.4	0.7	2.1
1163.00	Boomplaas Fm.	BP	Cr-red		0.5	5.3	1.9	4.3
1176.60	Boomplaas Fm.	BP	Bulk	0.37	0.3	6.2	2.9	4.7
1180.20	Boomplaas Fm.	BP	Bulk	0.39	0.3	7.2	3.5	5.5
1186.56	Vryburg Fm.	VB	Bulk	0.20	0.6	6.9	4.6	4.6
1187.70	Vryburg Fm.	VB	Bulk	0.17	0.1	2.1	0.8	1.6
1191.10	Vryburg Fm.	VB	Bulk	0.23	0.2	6.5	4.5	4.1
1195.90	Vryburg Fm.	VB	Bulk	0.19	0.5	5.7	4.1	3.6
1200.95	Vryburg Fm.	VB	Cr-red		1.1	3.3	2.9	1.8
1204.20	Vryburg Fm.	VB	Bulk	0.13	0.5	2.3	2.1	1.2
1206.17	Vryburg Fm.	VB	Bulk	0.16	0.8	2.3	1.4	1.5
1207.34	Vryburg Fm.	VB	Bulk	0.35	0.3	1.5	1.7	0.6
1209.40	Vryburg Fm.	VB	Bulk	0.20	0.3	2.2	2.4	0.9
1214.45	Vryburg Fm.	VB	Bulk	0.25	0.6	1.5	1.3	0.8
1220.20	Vryburg Fm.	VB	Bulk	0.17	0.7	2.6	2.3	1.5
1224.60	Vryburg Fm.	VB	Bulk	0.15	0.8	2.9	2.4	1.6
1231.00	Vryburg Fm.	VB	Bulk	0.15	0.3	2.2	1.7	1.4
1236.40	Vryburg Fm.	VB	Bulk	0.20	1.0	2.8	1.7	1.9
1272.10	Vryburg Fm.	VB	C0r-red		0.1	1.8	0.7	1.4
1277.40	Vryburg Fm.	VB	Bulk	0.11	0.2	3.3	1.2	2.7
1282.60	Vryburg Fm.	VB	Cr-red		0.2	1.0	1.5	0.2
1302.35	Vryburg Fm.	VB	Bulk	0.35	1.0	2.1	−0.3	2.2

[a] Bulk: analyzed by bulk combustion of acidified samples. Cr-red: analyses of Cr-reducible sulfur.
[b] Weight fraction loss by treatment with 6N HCl.
[c] Sulfur contents measured by XRF (Schröder et al., 2006).
[d] Tuff samples.

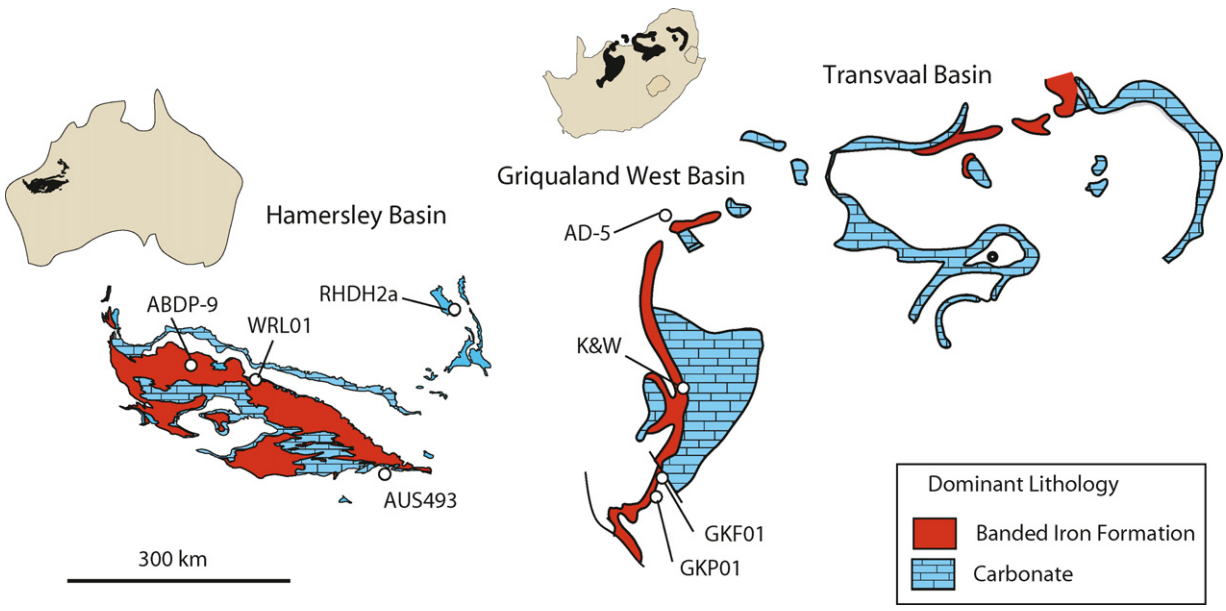

Fig. 1. Schematic map for the Hamersley Basin in Western Australia and Griqualand West and Transvaal Basins in South Africa. Locations for the studied cores (GKP01 and GKF01) are shown along with those used by previous studies.

temperature. Samples are then washed by deionized water and dried, and analyzed for their bulk $\delta^{34}S$ and $\Delta^{33}S$ values in the same manner as the Ag_2S isolates.

The Cr-reducible sulfur represent iron monosulfide and pyrite sulfur but the bulk combustion may include organic sulfur in addition to the Cr-reducible sulfur. Our dataset does not show significant isotopic difference between the two methods (Fig. 3), probably because of predominance of pyrite sulfur in given sample sets. Raw results were corrected for column drift and scale compression based on analyses of NBS 127, NZ1, and NZ3 international standards spaced through the analytical runs. Samples were measured in triplicate and averages of the measurements are reported. The uncertainty of $\delta^{34}S$ and $\Delta^{33}S$ by this EA-IRMS method is better than 0.3‰ (Kaufman et al., 2007).

4. Results and discussion

4.1. Geologic context of the Archean $\delta^{33}S$–$\delta^{34}S$ array

One of the most striking features of the Neoarchean multiple-sulfur isotope data is that some suites of samples yield a characteristic linear array with $\delta^{33}S \approx 1.4\ \delta^{34}S$ (i.e., $\Delta^{33}S \approx 0.89\ \delta^{34}S$) (Ono et al., 2003; Kaufman et al., 2007, Fig. 5C). This linear array was first measured in the lower Mt. McRae Shale in the drill

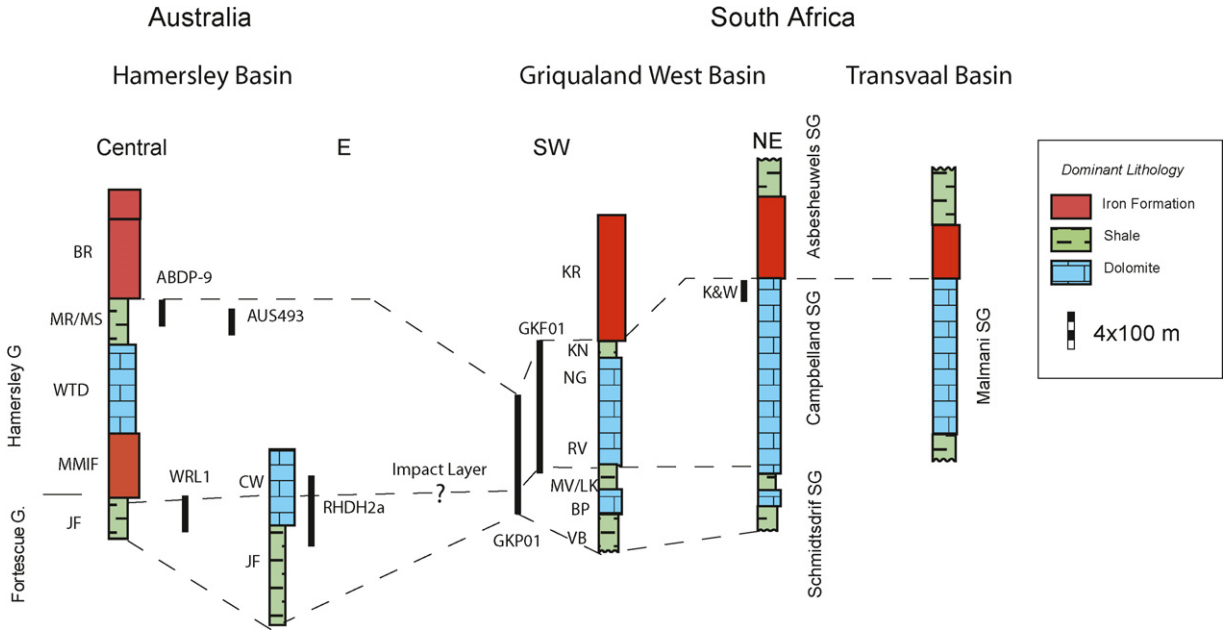

Fig. 2. General stratigraphy and correlation for the Neoarchean sequences in the Hamersley Basin, Western Australia and Griqualand West and Transvaal Basins, South Africa. Stratigraphic locations of the drill core materials used for this study (GKP01 and GKF01), as well as previous studies are shown. BR, Brockman Iron Formation; MR/MS, Mt. McRae Shale and Mt. Sylvia Formation; WTD, Wittenoom Dolomite; MMIF, Marra Mamba Iron Formation; JF, Jeerinah Formation; CW, Carawine Carbonate; KR, Kuruman Iron Formation; KN, Klein Naute Shale; NG, upper Nauga Formation; RV, Reivilo Formation; MV/LK, Monteville and Lokammona Formations; BP, Boomplaas Formation; and VB, Vryburg Formation.

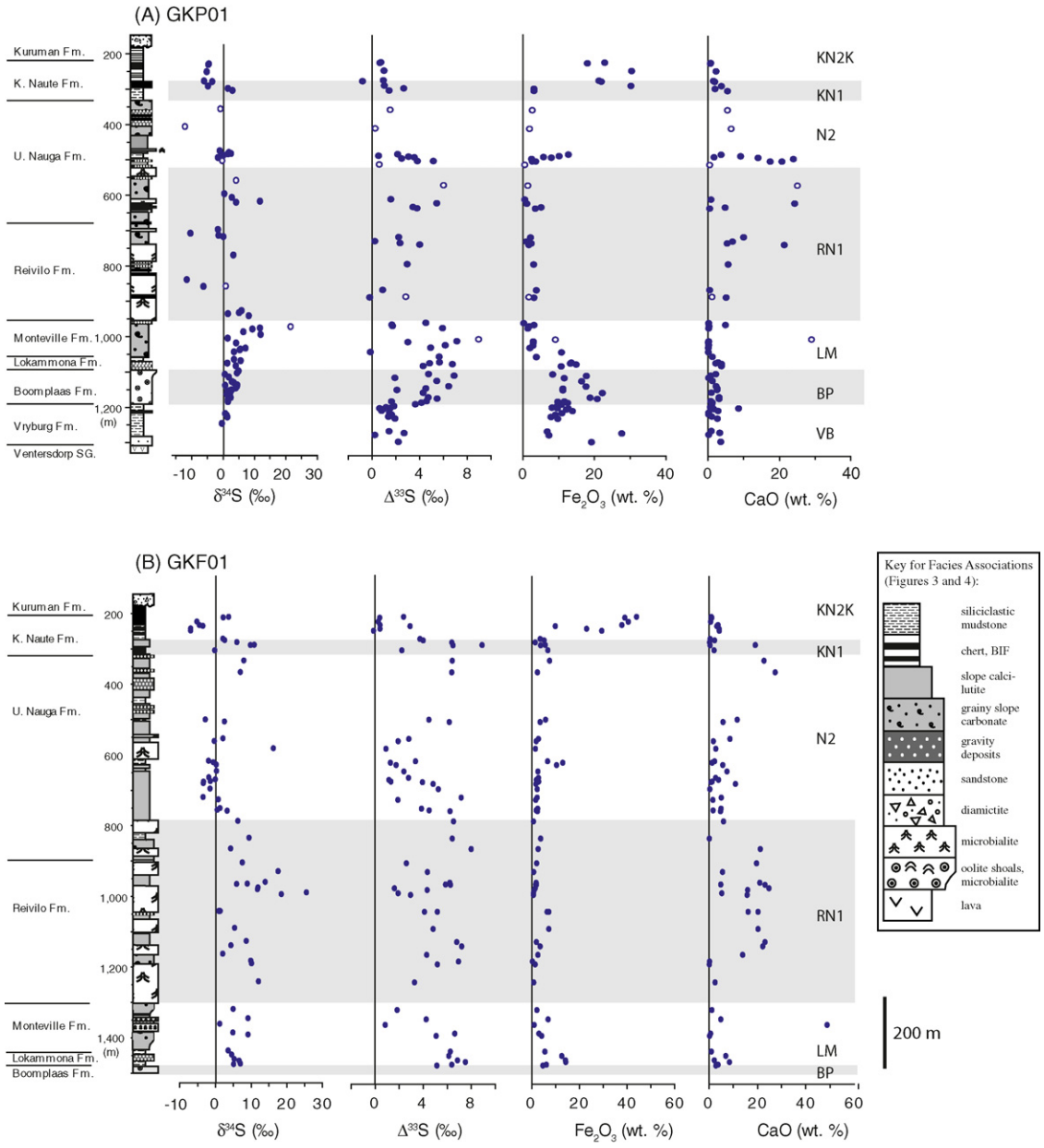

Fig. 3. Lithology and depth profile for sulfur isotope ratios and Fe_2O_3 and CaO contents of the cores GKP01 (A) and GKF01 (B). Open symbols in (A) are data for tuffs. Stratigraphic column is from Schröder et al. (2006).

core AUS493 (Ono et al., 2003). Recent high-resolution stratigraphic analysis by Kaufman et al. (2007) showed the identical relationship in the core, ABDP9, which is drilled ca. 300 km west from AUS493, suggesting that this slope is likely characteristic to the lower Mt. McRae Shale in the entire Hamersley Basin (Figs. 4 and 5C). A much smaller dataset presented by Kaufman et al. (2007) for South African Core (AD-5) also revealed a similar trend.

Data in some parts of the Agouron cores also plot along this linear trend, including the lowermost section of GKP01, including the Vryburg and the Boomplaas Formations (Fig. 4F and G). This is consistent with previous study of correlative sections in the Hamersley Basin, Australia, where some parts of the Jeerinah Formation yield a similar array of data (Ono et al., 2003). Thus, an emerging picture from the Neoarchean rock records is this linear trend is ubiquitous at both geographical (in two continents) and temporal (over 130 my) scales, and may reflect characteristic signature of atmospheric photochemistry of the Neoarchean Eon preserved in deep-time rock records (Ono et al., 2003; Kaufman et al., 2007).

The tight linear relationship, we call it the Archean reference array hereafter, may not be inherited directly from a specific MIF source reaction, such as SO_2 photolysis by <220 nm radiation. Instead, the array may be a mixing line between either two atmospheric sulfur reservoirs or atmospheric and ocean sulfur reservoirs. Farquhar and Wing (2003) noted that photolysis experiments using sulfur dioxide (e.g., Farquhar et al., 2000, 2001) did not provide a perfect match to the data in terms of $\delta^{33}S$ versus $\delta^{34}S$ relationships, but that laboratory experimental arrays for $\Delta^{36}S$ versus $\Delta^{33}S$ were similar to the observations. Ohmoto et al. (2006) have also noted that the lack of a perfect match between laboratory experiments and the observations argue against the atmospheric origin of the Archean S-MIF.

We have previously suggested that the linear correlation is a mixing array derived from Archean atmospheric S_8 aerosols (Ono et al., 2003). This is based upon results of photochemical model calculations that predict altitude variation in $\Delta^{33}S$ for atmospheric S_8; high-altitude S_8 carries large $\Delta^{33}S$ signature

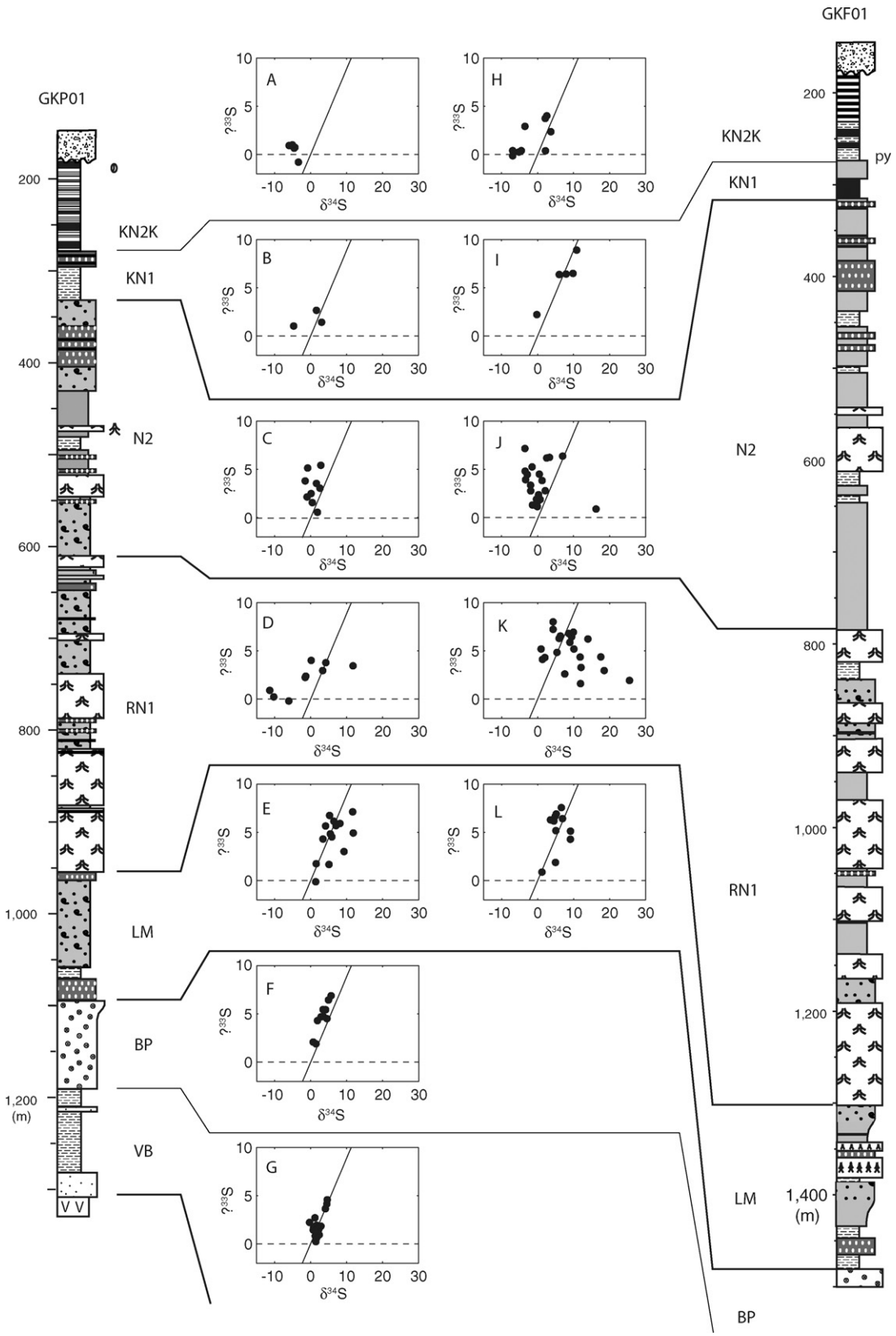

Fig. 4. $\delta^{34}S$ versus $\Delta^{33}S$ diagrams for subdivided sections of the cores. The solid lines are the Archean reference array ($\Delta^{33}S = 0.89\ \delta^{34}S$).

derived from photolysis of SO_2 and SO, whereas ground level S_8 carries small $\Delta^{33}S$ signatures due to isotope mixing with other sulfur gas species (Ono et al., 2003). The isotopic composition of the S_8 flux on the oceans would change as a function of the altitude of aerosol formation and precipitation (i.e., cloud formation).

The lower Mt. McRae Shale is a deepwater basinal facies, consisting of fine grain laminated pyritic and carbonaceous shale and

Table 2
Sulfur isotope data for the core GKF01.

Depth	Stratigraphy	Subdivision	Analysis	Acid loss	S (wt.%)	$\delta^{33}S$ (‰)	$\delta^{34}S$ (‰)	$\Delta^{33}S$ (‰)
207.90	Kuruman Fm.	KN2K	Bulk	0.64	0.3	4.3	3.7	2.4
209.80	Kuruman Fm.	KN2K	Bulk	0.61	0.2	1.5	2.2	0.4
221.65	Kuruman Fm.	KN2K	Bulk	0.63	0.4	−2.4	−5.2	0.3
231.00	Kuruman Fm.	KN2K	Bulk	0.60	0.5	−1.9	−4.5	0.4
233.95	K. Naute Fm.	KN2K	Bulk	0.36	5.6	1.1	−3.5	2.9
241.35	U. K. Naute Fm.	KN2K	Bulk	0.43	0.5	−3.2	−6.9	0.4
247.00	U. K. Naute Fm.	KN2K	Bulk	0.59	0.3	−3.7	−6.9	−0.1
270.10	U. K. Naute Fm.	KN2K	Bulk	0.03	0.3	4.8	2.1	3.7
274.03	U. K. Naute Fm.	KN2K	Bulk	0.09	1.0	5.3	2.6	4.0
280.00	L. K. Naute Fm.	NI	Bulk	0.02	0.5	9.5	6.0	6.4
287.60	L. K. Naute Fm.	NI	Bulk	0.69	0.7	14.5	10.8	8.9
288.10	L. K. Naute Fm.	NI	Bulk	0.02	0.8	11.6	9.9	6.5
302.75	U. Nauga Fm.	N2	Bulk	0.18	0.2	2.1	−0.2	2.2
331.90	U. Nauga Fm.	N2	Bulk	0.84	0.5	10.5	7.9	6.4
365.12	U. Nauga Fm.	N2	Bulk	0.91	0.2	10.0	7.0	6.4
499.40	U. Nauga Fm.	N2	Bulk	0.44	0.6	3.0	−2.9	4.5
505.76	U. Nauga Fm.	N2	Bulk	0.22	0.6	7.5	2.5	6.2
553.81	U. Nauga Fm.	N2	Bulk	0.33	0.4	3.9	2.1	2.8
560.48	U. Nauga Fm.	N2	Bulk	0.10	0.3	1.7	−0.3	1.9
581.82	U. Nauga Fm.	N2	Bulk	0.12	0.3	9.2	16.3	0.9
617.00	U. Nauga Fm.	N2	Bulk	0.16	0.2	2.4	−2.0	3.4
620.88	U. Nauga Fm.	N2	Bulk	0.24	0.3	1.0	−0.6	1.3
627.55	U. Nauga Fm.	N2	Bulk	0.17	0.4	1.9	0.3	1.8
645.71	U. Nauga Fm.	N2	Bulk	0.26	1.0	2.5	0.3	2.4
663.98	U. Nauga Fm.	N2	Bulk	0.14	0.6	1.8	−1.9	2.8
670.02	U. Nauga Fm.	N2	Bulk	0.18	0.3	1.1	−0.1	1.2
674.92	U. Nauga Fm.	N2	Bulk	0.07	0.6	0.6	−1.4	1.3
676.44	U. Nauga Fm.	N2	Bulk	0.05	0.3	2.2	−3.3	3.9
681.00	U. Nauga Fm.	N2	Bulk	0.38	0.4	3.1	−3.4	4.8
696.28	U. Nauga Fm.	N2	Bulk	0.05	0.3	4.5	−1.5	5.3
720.29	U. Nauga Fm.	N2	Bulk	0.21	0.2	5.4	−3.5	7.2
726.80	U. Nauga Fm.	N2	Bulk	0.18	1.0	2.3	0.8	1.9
751.52	U. Nauga Fm.	N2	Bulk	0.18	1.2	4.5	1.3	3.9
756.72	U. Nauga Fm.	N2	Bulk	0.07	0.5	4.8	0.5	4.5
759.13	U. Nauga Fm.	N2	Bulk	0.17	0.7	8.0	3.3	6.2
787.67	U. Nauga Fm.	RN1	Bulk	0.21	0.4	9.8	6.3	6.5
835.95	U. Nauga Fm.	RN1	Bulk	0.05	0.7	11.3	9.4	6.4
866.17	U. Nauga Fm.	RN1	Bulk	0.62	0.5	10.2	4.3	8.0
906.55	Reivilo Fm.	RN1	Bulk	0.59	0.4	6.5	7.5	2.6
930.70	Reivilo Fm.	RN1	Bulk	0.19	0.7	13.4	17.5	4.4
961.87	Reivilo Fm.	RN1	Bulk	0.81	0.3	13.4	14.0	6.2
966.23	Reivilo Fm.	RN1	Bulk	0.07	0.2	10.4	8.9	5.9
966.97	Reivilo Fm.	RN1	Bulk	0.87	0.3	9.3	6.0	6.3
976.94	Reivilo Fm.	RN1	Bulk	0.89	0.4	7.7	11.9	1.6
981.79	Reivilo Fm.	RN1	Bulk	0.52	0.5	10.4	11.8	4.3
991.53	Reivilo Fm.	RN1	Bulk	0.23	0.3	15.0	25.5	1.9
995.85	Reivilo Fm.	RN1	Bulk	0.50	0.2	12.4	18.5	2.9
1043.80	Reivilo Fm.	RN1	Bulk	0.65	0.3	5.7	1.0	5.2
1044.20	Reivilo Fm.	RN1	Bulk	0.71	0.3	4.8	1.3	4.1
1092.32	Reivilo Fm.	RN1	Bulk	0.50	0.3	7.6	5.4	4.8
1129.38	Reivilo Fm.	RN1	Bulk	0.89	0.3	11.2	8.6	6.8
1141.78	Reivilo Fm.	RN1	Bulk	0.60	0.8	9.4	4.3	7.2
1165.40	Reivilo Fm.	RN1	Bulk	0.78	0.4	5.3	2.0	4.3
1185.16	Reivilo Fm.	RN1	Bulk	0.02	0.3	12.0	9.9	6.9
1192.78	Reivilo Fm.	RN1	Bulk	0.03	0.4	10.4	10.1	5.2
1244.00	Reivilo Fm.	RN1	Bulk	0.10	0.4	9.5	12.0	3.3
1322.40	Monteville Fm.	LM	Bulk	0.07	0.3	4.4	5.0	1.8
1348.81	Monteville Fm.	LM	Bulk	0.22	0.4	8.9	9.1	4.2
1364.76	Monteville Fm.	LM	Bulk	0.97	0.6	1.5	1.2	0.8
1389.13	Monteville Fm.	LM	Bulk	0.04	0.4	9.2	4.9	6.6
1395.37	Monteville Fm.	LM	Bulk	0.07	0.2	9.8	9.2	5.1
1440.26	Lokammona Fm.	LM	Bulk	0.11	0.4	8.1	3.6	6.3
1452.33	Lokammona Fm.	LM	Bulk	0.32	0.2	8.5	4.5	6.1
1464.61	Lokammona Fm.	LM	Bulk	0.28	0.3	9.5	5.2	6.9
1469.45	Lokammona Fm.	LM	Bulk	0.39	0.4	10.9	6.6	7.5
1477.37	Lokammona Fm.	LM	Bulk	0.21	0.5	9.9	6.9	6.4
1479.80	Lokammona Fm.	LM	Bulk	0.13	0.3	7.8	5.1	5.1

sideritic banded iron formations that were deposited well below storm wave base. Thus, our previous study associated the linear correlation with deepwater basinal depositional environments (Ono et al., 2003). This association does not hold for the data presented here because the shallow water Boomplaas Formation yields a trend similar to that of the lower Mt. McRae Shale (Fig. 4F). The Boomplaas Formation from GKP01 is characterized by oolitic dolostones, and domal and columnar stromatolites, indicating a shallow subtidal environment above wave base (Beukes, 1987; Schröder et al., 2006). On the other hand, the upper Mt. McRae Shale is dominated by clastic carbonate and shale turbidites sourced from shallower water environments, and these samples do not follow the noted

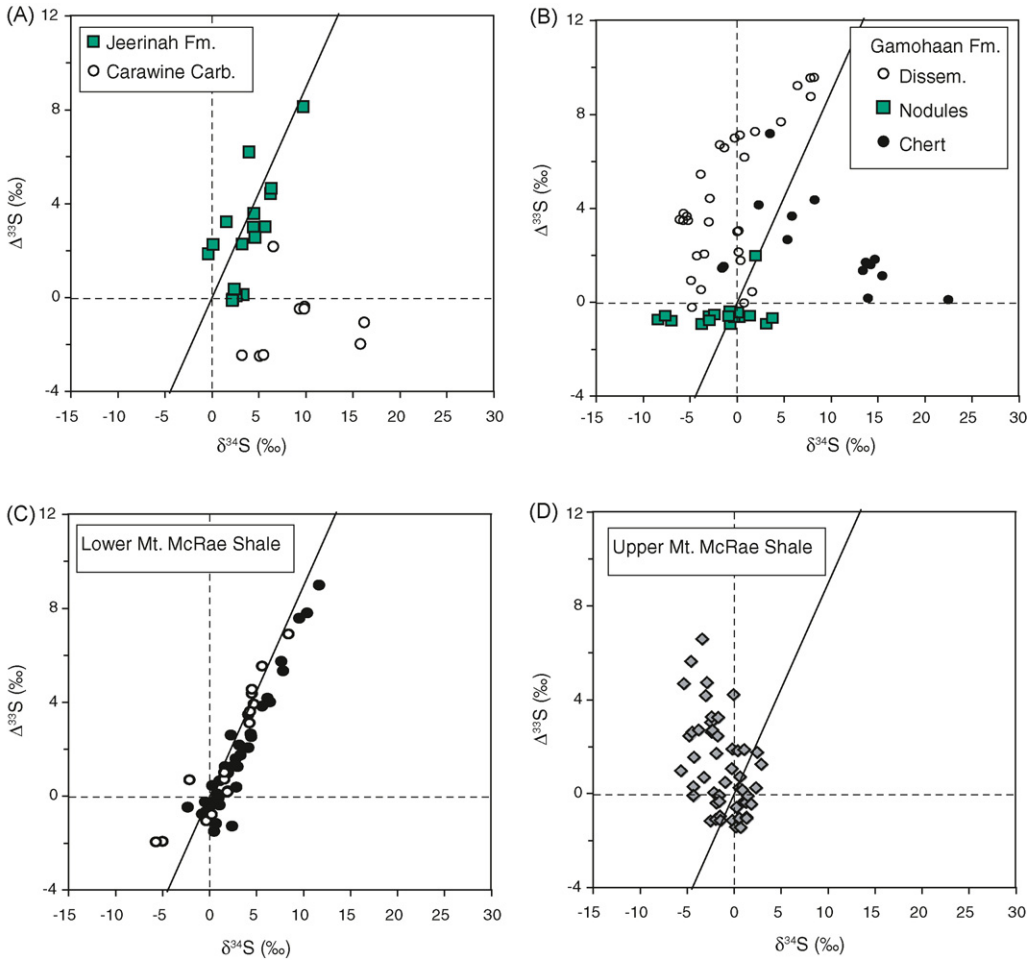

Fig. 5. Previously published data for the late Archean sedimentary sulfides. (A) 2.65 Ga Jeerinah Formation and Carawine Carbonate of the Hamersley Basin (Ono et al., 2003), (B) 2.5 Ga Gamohaan formation (Kamber and Whitehouse, 2007), and (C) 2.5 Ga lower Mt. McRae formation (open circles: Ono et al., 2003; solid circles: Kaufman et al., 2007), and (D) 2.5 Ga upper Mt. McRae formation of the Hamersley Basin.

sulfur isotope array. However the upper Mt. McRae Shale carbonates are lacking in iron, which may impose a critical chemical divide.

Instead of depositional environment, we relate the linear array in $\delta^{33}S$ and $\delta^{34}S$ to the chemistry of the shale because one of the common features of the lower Mt. McRae Shale and the shale in the Boomplaas and underlying the Vryburg formation are their high-iron contents (Fig. 3A, Schröder et al., 2006; Kaufman et al., 2007). The large positive $\Delta^{33}S$ values that lie on the Archean reference array were also measured from the ca. 170 m level of the ADBP-9 core (Kaufman et al., 2007). These are sideritic BIF and organic rich marl, characterized by high-iron contents (10–20 wt.% Fe; Anbar et al., 2007). Shales from the Boomplaas and Vryburg Formations of the GKP01 are also characterized by high-Fe contents (Fig. 3A; Schröder et al., 2006). Although the reactive Fe contents have not been measured for the cores GKP01 and GKF01, carbonate in the Boomplaas Formation is ferruginous, suggesting it was precipitated from iron-rich solutions (Beukes, 1987). Therefore, it appears that the preservation of S_8 signatures in the rock record may be related to the availability of Fe in the environments. Further study of Fe speciation (e.g., measurements of reactive Fe) may provide significant insights into Fe–S chemistry of the Neoarchean oceans. The preservation of the linear array (i.e., atmospheric signature) may well be related to the relative depth of Archean ocean chemoclines, which may have divided water masses of Fe^{2+}–H_2S, Fe^{2+}–O_2 or H_2S–O_2 pairs (Table 2).

4.2. Insights into Archean ocean Fe–S chemistry

The preservation of an atmospheric signature in Fe-rich rocks can be used to elucidate the chemistry of Archean oceans. Although a photochemical model calculations predict that H_2S was one of the dominant atmospheric sulfur species at ground level (e.g., Kasting et al., 1989), oceanic sulfide levels are generally thought to be low because its presence would result in the precipitation of highly insoluble iron sulfide minerals (e.g., Walker and Brimblecombe, 1985). Saito et al. (2003), however, suggested that Archean oceanic sulfides were predominantly in a form of relatively stable $FeSH^+$ complex based upon stability constants for metal sulfide complex obtained by electrochemical techniques. Assuming saturation with respect to $FeS_{(s)}$, the Archean $FeSH^+_{(aq)}$ level is solely a function of pH according to the reaction:

$$FeS_{(s)} + H^+ \rightarrow FeSH_{(aq)}{}^+ \quad (1)$$

The calculated total aqueous sulfide concentration is as high as 15 μmol/kg assuming ocean pH of 7.5 (Saito et al., 2003). In such a ferro-sulfidic Archean ocean, pyrite could have precipitated by reaction with atmosphere-derived S^0 though:

$$FeSH^+ + S^0 \rightarrow FeS_2 + H^+ \quad (2)$$

Here, the "zero valent sulfur (S^0)" is commonly used in the literature (e.g., Berner, 1970), but is a representation of an overall process (e.g., Rickard and Luther, 2007). The reaction (2) likely takes

place through polysulfide species (S_n^{2-}) and precipitation of pyrite (Schoonen and Barnes, 1991; Rickard and Luther, 2007), such as:

$$HS^- + S^0 \leftrightarrow S_n^{2-} + H^+ \quad (3)$$

and,

$$FeS + S_n^{2-} \rightarrow FeS_2 + S_{n-1}^{2-} \quad (4)$$

The reactions (1)–(4) do not produce large (>several ‰) mass-dependent isotope effects (e.g., Butler et al., 2004; Amrani et al., 2006). According to the reaction scheme (1) and (2), one of the sulfur atoms in pyrite comes from H_2S and the other from S^0. The kinetics of sulfur isotope exchange among reduced sulfur species (HS^-, S_n^{2-}, S^0 and $FeS_{(aq)}$), however, are rapid even at room temperatures, which may lead to identical isotope abundances (Fossing and Jorgensen, 1990; Amrani et al., 2006) such that they may have identical isotope compositions. These pathways may account for a significant part of the transfer of the ^{33}S-enriched sulfur to pyrite, and operation of reactions (1)–(4) in the water column or in surface sediments may determine the isotope signatures of the integrated HS^-–S^0–$FeS_{(aq)}$ pool.

4.3. Insights into microbial sulfate reduction in Neoarchean oceans

Following our model of the origin of the linear $\delta^{33}S$–$\delta^{34}S$ array, deviations from this array may serve as proxies for additional imprints by biologically mediated mass-dependent fractionation or inputs of sulfur from oceanic reservoir other than the HS^-–S^0–FeS pool, which is likely to be oceanic sulfate. Archean oceanic sulfate level was likely low, probably less than 200 μmol/kg (Habicht et al., 2002), but still was the most abundant aqueous sulfur species in the ocean. As pointed out by previous studies (Logan et al., 1995; Johnston et al., 2006; Kaufman et al., 2007), the behavior of sulfate in oceans with low sulfate concentrations may not be conservative, leading to lateral and vertical variations in sulfate concentration and isotopic composition. Such variations in sulfate concentration may also be reflected in the relationships between sulfur isotopic compositions and depositional facies. If microbial sulfate reduction occurred at the sediment–water interface rather than in the water column, the lower relative availability of sulfate coupled with high rates of sulfate reduction would lead to ^{34}S enrichment in sulfides as pore waters became progressively closed to the overlying water column (e.g., Ohmoto, 1992; Ohmoto and Goldhaber, 1997).

4.4. Pyrite-enriched in ^{34}S with respect to Archean reference array

Data from some sections of the cores are characterized by pyrite that is enriched in ^{34}S, and these data plot to the right of the reference linear array. This pattern is seen in section RN1 of GKF01 (Fig. 4K). Enriched ^{34}S values were previously found in pyrite grains in the Carawine Carbonate in the Hamersley Basin (Fig. 5A) and disseminated pyrite in chert from the Gamohaan Formation (Fig. 5B; Kamber and Whitehouse, 2007). Ono et al. (2003) interpreted the negative $\Delta^{33}S$ and positive $\delta^{34}S$ of pyrite from the Carawine Carbonate to reflect pyrite formed mostly from sulfide produced by microbial sulfate reduction of seawater sulfate because mass-dependent fractionation by microbial sulfate reduction would transfer the negative $\Delta^{33}S$ values of the Archean seawater sulfate into newly formed pyrite. In contrast, data from the section RN1 of GKF01 show enriched $\delta^{34}S$ accompanying positive $\Delta^{33}S$ values. This could point to either (1) Archean oceanic sulfate had heterogeneous $\Delta^{33}S$ values due to short residence time (Kaufman et al., 2007) or (2) the data reflect two-component mixing of sulfate-derived and S^0–H_2S-derived sulfide; the former has negative $\Delta^{33}S$ and positive $\delta^{34}S$ and the latter follows a linear array of $\delta^{33}S = \sim 1.4\,\delta^{34}S$. The small-scale (sub-cm) heterogeneity of $\Delta^{33}S$ values reported in Ono et al. (this volume) may support the latter possibility of local mixing of two sulfide components.

The Reivilo Formation in GKF01 is characterized by abundant microbialites, with textures suggesting abundant *in situ* carbonate precipitation on the seafloor (Sumner, 1997; Sumner and Grotzinger, 2004). Rapid cementation of sediments may have attenuated the supply of sulfate from seawater, resulting in progressive ^{34}S enrichments during bacterial sulfate reduction below the sediment–water interface. It is worth noting that data from the stratigraphically correlative section of RN1 in GKP01 plot left of the Archean reference array (Fig. 4D), which is consistent with a more abundant sulfate supply in relatively deeper depositional environment and a relatively later phase of cementation for the RN1 in GKP01.

4.5. Pyrite depleted in ^{34}S with respect to Archean reference array

Data that plot left of Archean reference array are seen in the upper Nauga Formations (N2) in both cores, as well as RN1 in GKP01 (Fig. 4C, D and J). The upper Nauga Formation is characterized by lumpy and laminated dolostones that are deposited on a slope that was a relatively deeper environment compared to the Reivilo Formation (Schröder et al., 2006). By extension of the above model, data with negative $\delta^{34}S$ can be mixtures of S_8-derived sulfur with sulfur-derived from open-system sulfate reduction. Relatively slower depositional rates of the upper Nauga Formation (with little direct seafloor carbonate precipitation) compared to the Reivilo section may lead to sulfate reduction in a relatively open environment. Relatively lower CaO contents in upper Nauga Formation samples (Fig. 3A and B) suggests that carbonate accumulation rates were low in this environment, which is consistent with more open-system exchange of sulfate between seawater and pore fluids.

The mixing (of sulfate- and S_8-derived sulfur) model is not a unique interpretation for the data that plot left of the Archean reference array. Philippot et al. (2007) attributed the microscopic pyrite in barite from the 3.5 Ga Dresser Formation as a signature of S^0 disproportionation. Although data presented in this study does not rule out either possibility, the presence or absence of sulfate reducers or sulfur disproportionators may have significant implications to early sulfur metabolisms and Archean ocean chemistry.

5. Conclusion

Time-series triple-sulfur isotope ratios $^{32}S/^{33}S/^{34}S$ for bulk rock samples were measured for two scientific cores that intersect the late Archean platform deposits of the Griqualand West Basin by a micro-combustion elemental analyzer-mass spectrometer. The $\Delta^{33}S$ ($\approx \delta^{33}S - 0.515\delta^{34}S$) values are positive except for three out of 141 samples, and range from −0.2 to +8.9‰ (average +2.9‰) and −0.1 to +8.9‰ (average +4.2‰) for GKP01 and GKF01, respectively.

In $\delta^{33}S$ and $\delta^{34}S$ plots, samples from the lowermost part of GKP01 (the Vryburg and Boomplaas Formations) and the uppermost parts of two cores (the Klein Naute and Kuruman Iron Formations) yield a linear array with $\delta^{33}S \approx 1.4\delta^{34}S$. This linear array is similar to those measured in the Neoarchean Hamersley Basin samples. Association of this linear array with iron rich rocks suggests the preservation of atmospheric S_8 signatures in the late Archean oceans that contained both iron and sulfides.

Some parts of the core showed deviation from the above reference array, representing local variations due to input of sulfide from microbial sulfate reduction. The enrichment or depletion of ^{34}S with respect to the reference array can be used to address openness of the system with respect to seawater sulfate. The closed system sulfate reduction is associated with a microbialite dominated

depositional environment, where drawdown of local sulfate would have been greatest and where direct precipitation of carbonate on the seafloor led to the closed-system sulfate reduction below the sediment water interface. Open-system sulfate reduction, in contrast, is associated with slope deposits where deepwater sources may have been more proximal and where carbonate cementation was not prevalent. Depositional and environment controls over multiple-sulfur isotope systematics were demonstrated for the Reivilo Formation, where GKP01 represents more distal facies compared to GKF01 and the isotopes behaved differently. The lateral variations in $\Delta^{33}S$–$\delta^{34}S$ systematics documented by this study may complicate the interpretation of strategraphic trends and their implication to the Neoarchean rise of oxygen. Further documentation of high-resolution analysis coupled with iron speciation will provide detailed understanding of the Archean sulfur cycles and the protracted history of Earth's atmospheric oxygenation during the Neoarchean Eon.

Acknowledgements

The authors thank J. Kirschvink, J. Grotzinger, and A. Knoll for formulating the South African drilling project and the Agouron Institute for funding this unique opportunity. Additional funding came from NASA Astrobiology Institute to SO, JF, NASA Exobiology to DYS (NAG5-10591 and NNG04GJ12G) and SO (NNX07AUG12G), AJK, and JF, and NSF-EAR to JF and AJK. We also thank B. Guy, N. Collins, and K. Yokoyama for assistance in sample preparation and analysis.

References

Amrani, A., Kamyshny, A., Lev, O., Aizenshtat, Z., 2006. Sulfur stable isotope distribution of polysulfide anions in an $(NH_4)_2S_n$ aqueous solution. Inorganic Chemistry 45, 1427–1429.

Anbar, A.D., Duan, Y., Lyons, T.W., Arnold, G.L., Kendall, B., Creaser, R.A., Kaufman, A.J., Gordon, G.W., Scott, C., Garvin, J., Buick, R., 2007. A whiff of oxygen before the great oxidation event? Science 317, 1903–1906.

Armstrong, R.A., Compston, W., Retief, E.A., Wilke, N.J., 1986. Ages and isotopic evolution of the Ventersdorp volcanics. Extended Abstract. Geocongress 1986. Geological Society of South Africa, pp. 89–92.

Barton, E.S., Altermann, W., Williams, I.S., Smith, C.B., 1994. U–Pb zircon age for a tuff in the Campbell Group, Griqualand West Sequence South Africa; implications for early Proterozoic rock accumulation rates. Geology 22, 343–346.

Baublys, K.A., Golding, S.D., Young, E., Kamber, B.S., 2004. Simultaneous determination of $\delta^{33}S$(V-CDT) and $\delta^{34}S$(V-CDT) using masses 48, 49 and 50 on a continuous flow isotope ratio mass spectrometer. Rapid Communications in Mass Spectrometry 18, 2765–2769.

Bekker, A., Holland, H.D., Wang, P.L., Rumble, D., Stein, H.J., Hannah, J.L., Coetzee, L.L., Beukes, N.J., 2004. Dating the rise of atmospheric oxygen. Nature 427, 117–120.

Berner, R.A., 1970. Sedimentary pyrite formation. American Journal of Science 268, 1–23.

Beukes, N.J., 1987. Facies relations, depositional environments and diagenesis in a major early Proterozoic stromatolitic carbonate platform to basinal sequence, Campbellrand Subgroup, Transvaal Supergroup Southern Africa. Sedimentary Geology 54, 1–46.

Butler, I.B., Bottcher, M.E., Rickard, D., Oldroyd, A., 2004. Sulfur isotope partitioning during experimental formation of pyrite via the polysulfide and hydrogen sulfide pathways: implications for the interpretation of sedimentary and hydrothermal pyrite isotope records. Earth and Planetary Science Letters 228, 495–509.

Eigenbrode, J.L., Freeman, K.H., 2006. Late Archean rise of aerobic microbial ecosystems. In: Proceedings of the National Academy of Sciences of the United States of America, vol. 103, pp. 15759–15764.

Farquhar, J., Bao, H.M., Thiemens, M., 2000. Atmospheric influence of Earth's earliest sulfur cycle. Science 289, 756–758.

Farquhar, J., Savarino, J., Airieau, S., Thiemens, M.H., 2001. Observation of wavelength-sensitive mass-independent sulfur isotope effects during SO_2 photolysis: implications for the early atmosphere. Journal of Geophysical Research 106, 1–11.

Farquhar, J., Wing, B.A., 2003. Multiple sulfur isotopes and the evolution of the atmosphere. Earth and Planetary Science Letters 213, 1–13.

Fossing, H., Jorgensen, B.B., 1990. Isotope exchange-reactions with radiolabeled sulfur-compounds in anoxic seawater. Biogeochemistry 9, 223–245.

Habicht, K.S., Gade, M., Thamdrup, B., Berg, P., Canfield, D.E., 2002. Calibration of sulfate levels in the Archean Ocean. Science 298, 2372–2374.

Hsieh, Y.P., Yang, C.H., 1989. Diffusion methods for the determination of reduced inorganic sulfur species in sediments. Limnology and Oceanography 34, 1126–1130.

Johnston, D.T., Poulton, S.W., Fralick, P.W., Wing, B.A., Canfield, D.E., Farquhar, J., 2006. Evolution of the oceanic sulfur cycle at the end of the Paleoproterozoic. Geochimica et Cosmochimica Acta 70, 5723–5739.

Kamber, B.S., Whitehouse, M.J., 2007. Micro-scale sulphur isotope evidence for sulphur cycling in the late Archean shallow ocean. Geobiology 5, 5–17.

Kasting, J.F., Zahnle, K.J., Pinto, J.P., Young, A.T., 1989. Sulfur, ultraviolet radiation, and the early evolution of life. Origins of Life and Evolution of the Biosphere 19, 95–108.

Kaufman, A.J., Johnston, D.T., Farquhar, J., Masterson, A.L., Lyons, T.W., Bates, S., Anbar, A.D., Arnold, G.L., Garvin, J., Buick, R., 2007. Late Archean biospheric oxygenation and atmospheric evolution. Science 317, 1900–1903.

Logan, G.A., Hayes, J.M., Hieshima, G.B., Summons, R.E., 1995. Terminal Proterozoic reorganization of biogeochemical cycles. Nature 376, 53–56.

Ohmoto, H., 1992. Biogeochemistry of sulfur and the mechanisms of sulfide–sulfate mineralization in Archean oceans. In: Schidlowski, M. (Ed.), Early Organic Evolution: Implications for Mineral and Energy Resources. Springer-Verlag, pp. 378–397.

Ohmoto, H., Goldhaber, M.B., 1997. Sulfur and carbon isotopes. In: Barnes, H.L. (Ed.), Geochemistry of Hydrothermal Ore Deposits. John Wiley & Sons, New York.

Ohmoto, H., Watanabe, Y., Ikemi, H., Poulson, S.R., Taylor, B.E., 2006. Sulphur isotope evidence for an oxic Archaean atmosphere. Nature 442, 908–911.

Ono, S., Eigenbrode, J.L., Pavlov, A.A., Kharecha, P., Rumble, D., Kasting, J.F., Freeman, K.H., 2003. New insights into Archean sulfur cycle from mass-independent sulfur isotope records from the Hamersley Basin, Australia. Earth and Planetary Science Letters 213, 15–30.

Pavlov, A.A., Kasting, J.F., 2002. Mass-independent fractionation of sulfur isotopes in Archean sediments: strong evidence for an anoxic Archean atmosphere. Astrobiology 2, 27–41.

Philippot, P., Van Zuilen, M., Lepot, K., Thomazo, C., Farquhar, J., Van Kranendonk, M.J., 2007. Early Archaean microorganisms preferred elemental sulfur, not sulfate. Science 317, 1534–1537.

Rickard, D., Luther, G.W., 2007. Chemistry of iron sulfides. Chemical Reviews 107, 514–562.

Saito, M.A., Sigman, D.M., Morel, F.M.M., 2003. The bioinorganic chemistry of the ancient ocean: the co-evolution of cyanobacterial metal requirements and biogeochemical cycles at the Archean–Proterozoic boundary? Inorganica Chimica Acta 356, 308–318.

Schoonen, M.A.A., Barnes, H.L., 1991. Reactions forming pyrite and marcasite from solution: II Via FeS precursors below 100[degree sign]C. Geochimica et Cosmochimica Acta 55, 1505–1514.

Schröder, S., Lacassie, J.P., Beukes, N.J., Gutzmer, J., de Kock, M., van Niekerk, H., Simonson, B.M., 2006. Stratigraphic and geochemical framework of the Agouron drill cores, Transvaal Supergroup (Neoarchean–Paleoproterozoic South Africa). South African Journal of Geology 109, 23–54.

Sumner, D.Y., 1997. Carbonate precipitation and oxygen stratification in late Archean seawater as deduced from facies and stratigraphy of the Gamohaan and Frisco Formations, Transvaal Supergroup South Africa. American Journal of Science 297, 455–487.

Sumner, D.Y., Beukes, N.J., 2006. Sequence stratigraphic development of the Neoarchean Transvaal carbonate platform, Kaapvaal Craton South Africa. South African Journal of Geology 109, 11–22.

Sumner, D.Y., Bowring, S.A., 1996. U–Pb geochronologic constraints on deposition of the Campbellrand Subgroup, Transvaal Supergroup South Africa. Precambrian Research 79, 25–35.

Sumner, D.Y., Grotzinger, J.P., 2004. Implications for Neoarchaean ocean chemistry from primary carbonate mineralogy of the Campbellrand-Malmani Platform South Africa. Sedimentology 51, 1273–1299.

Walker, J.C.G., Brimblecombe, P., 1985. Iron and sulfur in the pre-biologic ocean. Precambrian Research 28, 205–222.

Walraven, F., Martini, J., 1995. Zircon Pb-evaporation age determinations of the Oak Tree Formation, Chuniespoort Group Transvaal Sequence: implications for Transvaal-Griqualand West Basin correlations. South African Journal of Geology 98, 58–67.